JCTC Journal of Chemical Theory and Computation

Rigid-Body Molecular Dynamics of Fullerene-Based Nanocars on Metallic Surfaces

Sergei S. Konyukhov,[†] Ilya V. Kupchenko,[†] Alexander A. Moskovsky,[†] Alexander V. Nemukhin,[†,‡] Alexey V. Akimov,[§] and Anatoly B. Kolomeisky*[,§]

Department of Chemistry, M.V. Lomonosov Moscow State University, Leninskie Gory 1/3, Moscow 119991, and N.M. Emanuel Institute of Biochemical Physics, Russian Academy of Sciences, ul. Kosygina 4, Moscow 119994, Russian Federation, and Department of Chemistry, Rice University, Houston, Texas 77005

Received February 19, 2010

Abstract: Methodical problems of coarse-grained-type molecular dynamics, namely, rigid-body molecular dynamics (RB MD), are studied by investigating the dynamics of nanosized molecular vehicles called nanocars that move on gold and silver surfaces. Specifically, we analyzed the role of thermostats and the effects of temperature, couplings, and correlations between rigid fragments of the nanocar molecule in extensive RB MD simulations. It is found that the use of the Nosé−Poincaré thermostat does not introduce systematic errors, but the time trajectories might be required to be limited to not accumulate large numerical integration errors. Correlations in the motion of different fragments of the molecules are also analyzed. Our theoretical computations also point to the importance of temperature, interfragment interactions, and interactions with surfaces and to the nature of the surface for understanding mechanisms of motion of single-molecule transporters.

1. Introduction

Computer simulations based on molecular dynamics (MD) methods are critically important for understanding mechanisms of fundamental processes. MD is a powerful and convenient tool for analyzing different biological and chemical systems such as protein folding phenomena, motor protein dynamics, and transport across channels and membranes. Recently, MD methods have also been applied for studying artificial molecular motors, rotors,[1−8] and single-molecule transporters that include nanocars.[9−17]

In principle, classical MD methods are based on solving equations of motion for every atom of the system at all times, and this allows visualization and prediction of the dynamics of the system at the molecular level. However, a real system has a very large number of particles and degrees of freedom, and it becomes prohibitively expensive to solve these equations and to get a reasonable description of the system. It is known that full atomic MD simulations cannot capture processes that involve large groups of atoms for times longer than hundreds of nanoseconds, while typical chemical and biological time scales range from 1 ms to 1 min. In addition, in many systems some degrees of freedom are less important than others for dynamical properties. These considerations stimulated a development of the so-called coarse-grained MD methods in which groups of atoms are viewed as new "effective" particles and some degrees of freedom are ignored. These approaches significantly accelerate computations by decreasing the number of particles and/or degrees of freedom. However, this raises an important question on how realistic these coarse-grained descriptions of the studied phenomenon are.

The goal of this study is to analyze the applicability of a version of coarse-grained MD for analyzing single-molecule dynamics. Specifically, we will study recently developed rigid-body molecular dynamics (RB MD) methods[18−24] that have been successfully applied for studying complex dynamics of artificial molecular motors (nanocars)[17] and molecular rotors.[25−29] Using this approach, many important details of

* Corresponding author phone: (713) 348-5672; e-mail: tolya@rice.edu.

[†] M.V. Lomonosov Moscow State University.

[‡] Russian Academy of Sciences.

[§] Rice University.

10.1021/ct100101y
Published on Web 07/30/2010

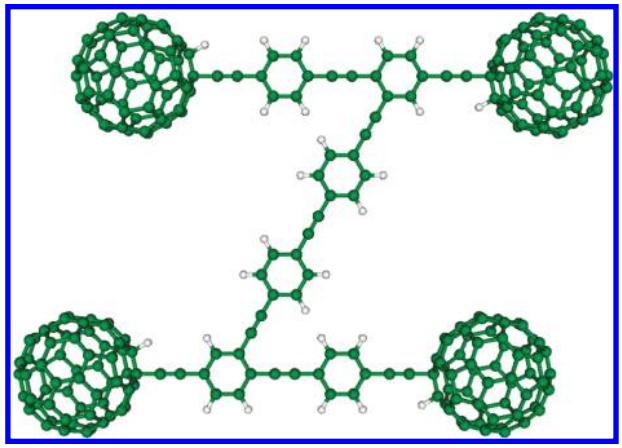

Figure 1. Model of the z-car with four fullerene wheels chemically bound to a chassis.

the molecular motion at the nanoscale have been uncovered. It also allowed us to better understand recent single-molecule measurements on molecular motors and rotors. In RB MD the molecules are viewed as collections of rigid fragments; i.e., many vibrational and rotational degrees of freedom are neglected. Since RB MD provides a reasonable description of the dynamics of nanocars on metallic surfaces, as compared with experiments, we have chosen this system as our testing ground for checking the reliability of RB MD calculations. By performing extensive numerical simulations, we analyze the effect of using a specific Nosé−Poincaré thermostat[30−34] and the effect of temperature, correlations, molecular flexibility, and interactions between different parts of the system. There are several types of nanocar molecules that have been synthesized in recent years. In our work the dynamics of a single molecule, known as a z-car and shown in Figure 1, is studied on gold and silver surfaces because of the high stability of this molecule on these surfaces.

It should be noted that the development of a realistic RB MD tool is also very important for practical applications. It will allow us to better understand mechanisms of motion on the surface by single-molecule transporters, and it will help to create efficient nanoscale transport systems capable of performing useful work at the molecular level.

2. Methods

To test the RB MD method, we used a simplified model of the dynamics of the z-car molecule (illustrated in Figure 1) on gold and silver surfaces under conditions close to vacuum which are similar to what is observed in experiments.[12] The original z-car molecule has several tail fragments that increase its solubility in organic solvents and make the molecule more rigid. In our computations we used a smaller molecule without tails to have a more comprehensive description of the system dynamics. In further discussions, we call this simplified version a z-car molecule.

The molecules move along the metal surface, which is viewed as an ideal two-dimensional square-lattice plane with the lattice parameters equal to 4.07 Å for gold and 4.08 Å for silver. Our main assumption here is that the metal lattice is rigid and interactions with the z-car do not change the underlying lattice geometry of the surface. Effectively, this

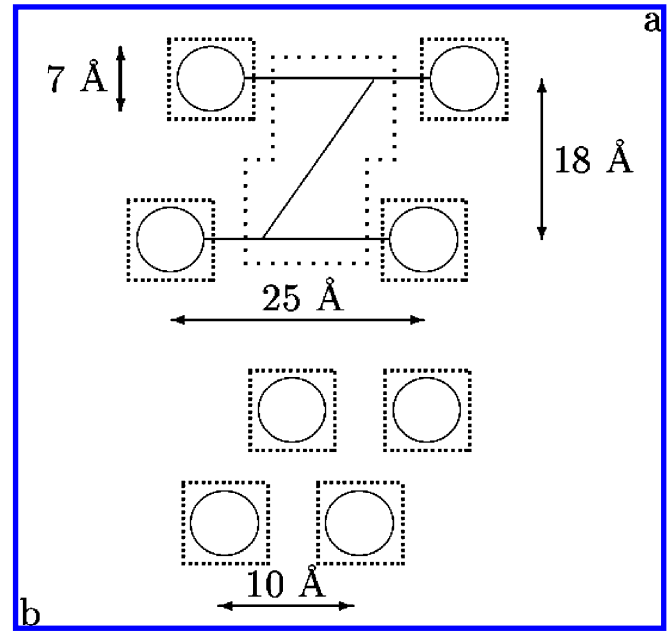

Figure 2. Partitioning the model systems into fragments: (a) z-car, (b) four wheels (4 × C_{60}).

corresponds to taking into account only the upper surface atom layer although the effect of the bottom levels has been analyzed as well.

The structure of the z-car molecule suggests that it is reasonable to divide it into five rigid segments: four corresponding to the wheels and one to the chassis. Since we are interested in correlations and interactions between different parts of the z-car molecule, for comparison we also analyzed the molecular dynamics of a separate system consisting of only four fullerene wheels moving on the same surfaces. Schematic pictures of the considered particles and their geometries are presented in Figure 2.

The crucial part of any MD calculation is the potential energy. Most of the parameters for the present simulations have been taken from the CHARMM27 force field[35,36] augmented by those from the UFF parameter set.[37] Interactions with silver atoms have been parametrized[38] to reproduce the adsorption energies of some relatively small molecules, such as fullerenes. Since charge transfer processes might play a significant role in interactions between fullerenes and metallic surfaces,[39−43] this procedure allowed us to take into account, at least partially, various chemisorption effects. The overall potential energy is additive, and it can be written in the following form:

$$E = E_{\text{bond}} + E_{\text{angle}} + E_{\text{vdw}} + E_{\text{Coulomb}} + E_{\text{surface-molecule}} \quad (1)$$

The first term describes the radial part of the covalent bond interaction:

$$E_{\text{bond}} = \sum_{\text{bonds}} kb_i(r_i - r_i^{\text{eq}})^2 \quad (2)$$

where r_i and r_i^{eq} are the length and the equilibrium length, respectively, of bond i. The second term in eq 1 corresponds to the angular contribution to the interactions:

$$E_{\text{angle}} = \sum_{\text{angles}} ka_i(\varphi_i - \varphi_i^{\text{eq}})^2 \quad (3)$$

where φ_i and φ_i^{eq} are the angle and the equilibrium angle, respectively, between two neighboring bonds. In our calculations the effect of torsion interactions has been mostly ignored. The third term in eq 1 describes the noncovalent interactions in the system that are assumed to be of the standard Lennard-Jones type:

$$E_{\text{vdw}} = \sum_{i,j} \varepsilon_{ij}\left[\left(\frac{r_{ij}^0}{r_{ij}}\right)^{12} - 2\left(\frac{r_{ij}^0}{r_{ij}}\right)^{6}\right] \quad (4)$$

where $\varepsilon_{ij} = (\varepsilon_i\varepsilon_j)^{1/2}$ and r_{ij} is the distance between atoms i and j. The fourth term in eq 1 corresponds to electrostatic interactions:

$$E_{\text{Coulomb}} = \sum_{i<j}\left(\frac{q_i q_j}{r_{ij}}\right) \quad (5)$$

where q_i is the charge on atom i. This contribution was neglected for the case of the Au surface. However, the effect of the charge transfer in the case of the Ag surface was implicitly taken into account in the utilized potential.[38] Finally, the last term represents the interaction between the molecule and the surface. For the Au surface it was taken to be of the Lennard-Jones type, while for the Ag surface a Morse potential has been used. In our calculations on the gold surface, we explicitly considered noncovalent interactions with the 625 closest surface gold atoms. Note also that we took into account van der Waals interactions between different parts of the z-car molecule. For the silver surface we considered explicitly interactions with the 2134 closest surface atoms.

MD simulations have been performed with the help of the Nosé−Poincaré thermostat[30−34] at $T = 300$ K for dynamics on the gold surface and for the range of temperatures between 200 and 600 K for the motion of z-car molecules on the silver surface. We have used for simulation two computer codes that were independently developed in our groups. The length of each trajectory was 20 ns for the dynamics on gold and 1 ns for the silver surface with a time step of 1 fs. All obtained dynamic properties have been averaged over 48 trajectories for Au and over 10−30 trajectories (at each temperature) for the Ag surface.

3. Results and Discussion

3.1. Evaluation of the Thermostat. A crucial element in our RB MD simulations is utilization of the Nosé−Poincaré thermostat, and it is important to understand its advantages and limitations. One of the special properties of this thermostat that distinguishes it from other thermostats is that the dynamics produced with the help of the Nosé−Poincaré thermostat is Hamiltonian. This observation allowed us to control, at least partially, the quality of numerical integrations of equations of motion by monitoring a special function called the Nosé−Poincaré invariant, $H_{\text{N-P}}$, which corresponds exactly to a Hamiltonian function of another system that approximates the dynamics in the given system. The quality of the calculations can be judged by analyzing the invariant as a function of time. Deviations can be approximated as a linear function:

$$H_{\text{N-P}}(t) = At + B \quad (6)$$

The dependence of invariants as a function of time for MD simulations on a gold surface is shown in Figure 3. In addition, Table 1 provides information, averaged over all trajectories, for the absolute values of $H_{\text{N-P}}$ and also for coefficients A and B. It can be seen that all these parameters are similar in value with absolute errors, and one might conclude that the algorithm of numerical integration of the equations of motion used in our RB MD simulations does not produce systematic errors. In addition, it could be noted that if the trend in the invariant does not change, then we can estimate the maximal allowed time length, $t_{\max}$, of trajectories in our method by comparing the deviations of the invariant and typical interaction energies in the system (∼1 kcal/mol). In this system it is equal to ∼10 ns. Thus, there are situations when longer trajectories might not be as precise in measuring system dynamics. However, this observation strongly depends on the time-dependent behavior of the invariant, and it should be carefully checked in all systems. Our calculations on a Ag surface suggest that preliminary equilibration of the structure might decrease the trend in the invariant, and longer trajectories (up to 1 ms) could be used for analyzing the dynamics of nanocars. It should be noted also that in our analysis of correlations we included the initial time segments to have the most conservative estimate of the parameters of the system. Removing the initial times might significantly improve the computer simulation results.

Another way of checking the quality of the utilized thermostat is to analyze how it reproduces the properties of the canonical ensemble. This is related to the problem of ergodicity for trajectories obtained with the help of the Nosé−Poincaré thermostat. It is convenient to view the kinetic energy of the system as a proper characteristic property for reproducing canonic ensemble properties. The kinetic energy can be written as the sum of translational and rotational contributions for each fragment:

$$E_{\text{kin}} = \sum_{\text{fragments}} (E_{\text{kin}}^{\text{trans}} + E_{\text{kin}}^{\text{rot}}) \quad (7)$$

In this equation we have

$$E_{\text{kin}}^{\text{trans}} = \frac{1}{2m}(p_{\text{trans},x}{}^2 + p_{\text{trans},y}{}^2 + p_{\text{trans},z}{}^2) \quad (8)$$

where m is the mass of the fragment and $p_{\text{trans},i}$ are projections of the translational momentum on axis i. Similarly for the rotational kinetic energy

$$E_{\text{kin}}^{\text{rot}} = \frac{p_{\text{rot},x}{}^2}{2I_x} + \frac{p_{\text{rot},y}{}^2}{2I_y} + \frac{p_{\text{rot},z}{}^2}{2I_z} \quad (9)$$

where $p_{\text{rot},i}$ are projections of rotational momentum and $I_{x,y,z}$ are the moments of inertia in the system. In the canonical

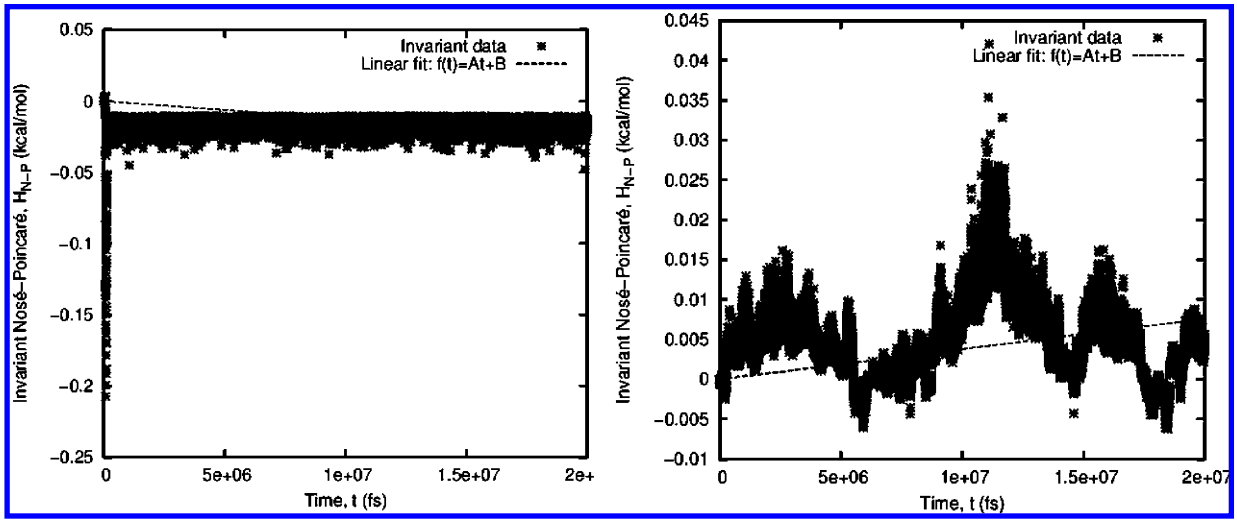

Figure 3. Time dependence of the Nosé−Poincaré invariant for 4 × C_{60} (left) and z-car (right) on a gold surface.

Table 1. Nosé−Poincaré Invariant Values, H_{N-P}, and the Coefficients of the Linear Approximation (Eq 6) of the Trend

system	$H_{N-P} \pm \Delta H_{N-P}$, kcal/mol	$A \pm \Delta A$, (kcal/mol) fs^{-1}	$B \pm \Delta B$, kcal/mol
4 × C_{60}	$(4 \pm 2) \times 10^{-2}$	$(-3 \pm 5) \times 10^{-8}$	$(4 \pm 2) \times 10^{-2}$
z-car	$(3 \pm 2) \times 10^{-3}$	$(3 \pm 2) \times 10^{-7}$	$(-1 \pm 1) \times 10^{-4}$

ensemble the probabilities for all moments follow a Boltzmann distribution:

$$f(p) = A_f p_r^2 \exp\left[-\frac{p_r^2}{B_f}\right] \tag{10}$$

where p_r is the reduced moment given by

$$p_r = \frac{p_{trans,j}}{m} \quad \text{or} \quad p_r = \frac{p_{rot,j}}{\sqrt{I_j}} \qquad j = x, y, z \tag{11}$$

and the coefficients A_f and B_f are equal to

$$A_f = \frac{4}{\sqrt{\pi}}\left(\frac{1}{2k_BT}\right)^{-3/2} \qquad B_f = 2k_BT \tag{12}$$

The distributions obtained in our MD simulations are compared with distributions theoretically calculated via eq 10 in Figures 4 and 5.

The results of our simulations reproduce quite well theoretical distributions for the system of four fullerene wheels and for the wheels in the z-car. However, some deviations are observed for the chassis of the z-car. Most probably this is related to deviations from ergodicity for the results obtained with the Nosé−Poincaré thermostat. The chassis of the z-car molecules is strongly limited in its motion by coupling to the fullerene wheels, and probably it does not help to explore fully the phase space of the system to satisfy the Boltzmann distribution.

3.2. Correlations in the Motion of Fullerene Wheels. Our previous studies have shown that rotation of the wheels is a dominating factor in the mobility of nanocars.[24] To understand the mechanism of the motion of these molecules, it is important to estimate correlations in the wheel rotations. To do this, we compared the motion of the z-car molecule with the dynamics of a system consisting of only four fullerene wheels. Our MD simulations indicate that if we position four fullerene wheels like in the z-car molecule, then after some time they come together and stay as one dynamic cluster with a distance between neighboring fullerenes on the order of 1 nm. This is due to van der Waals interactions between the particles. For the z-car, these interactions between the wheels are very weak and fullerenes do not directly affect each other. Any possible correlations are the result of the effective interactions with the whole system.

To quantify rotational correlations, we introduce several functions that we might call correlation functions. Specific values for these functions, as described below, will provide a relative measure of the correlations. First, we define a function C

$$C = \frac{2}{3}\frac{\sum_{i<j}(\mathbf{w}_i\mathbf{w}_j)}{\sum_i(\mathbf{w}_i\mathbf{w}_i)} \tag{13}$$

where $(\mathbf{w}_i\mathbf{w}_j)$ is a scalar product of two angular velocity vectors for wheels i and j. The physical meaning of this function is the following. If the absolute values and directions of all angular velocities are the same, i.e., the case of very strong correlations, the value of this function is equal to 1. If the motion of the wheel is uncorrelated, the value of the function C should be between 0 and −1/3. The last value, for example, can be obtained in the case where the absolute values of all angular velocities are the same and two vectors are in the upper direction while two other vectors are in the opposite direction.

The function C provides a measure of both correlations in the direction and in the absolute values of the rotational speeds of the wheels. We also introduce two other functions, C_{dir} and C_{abs}, that are more specific indicators of the corresponding correlations:

$$C_{dir} = \frac{1}{4}\sum_{i=1}^{4}(\mathbf{n}_i\mathbf{n}_{av}) \tag{14}$$

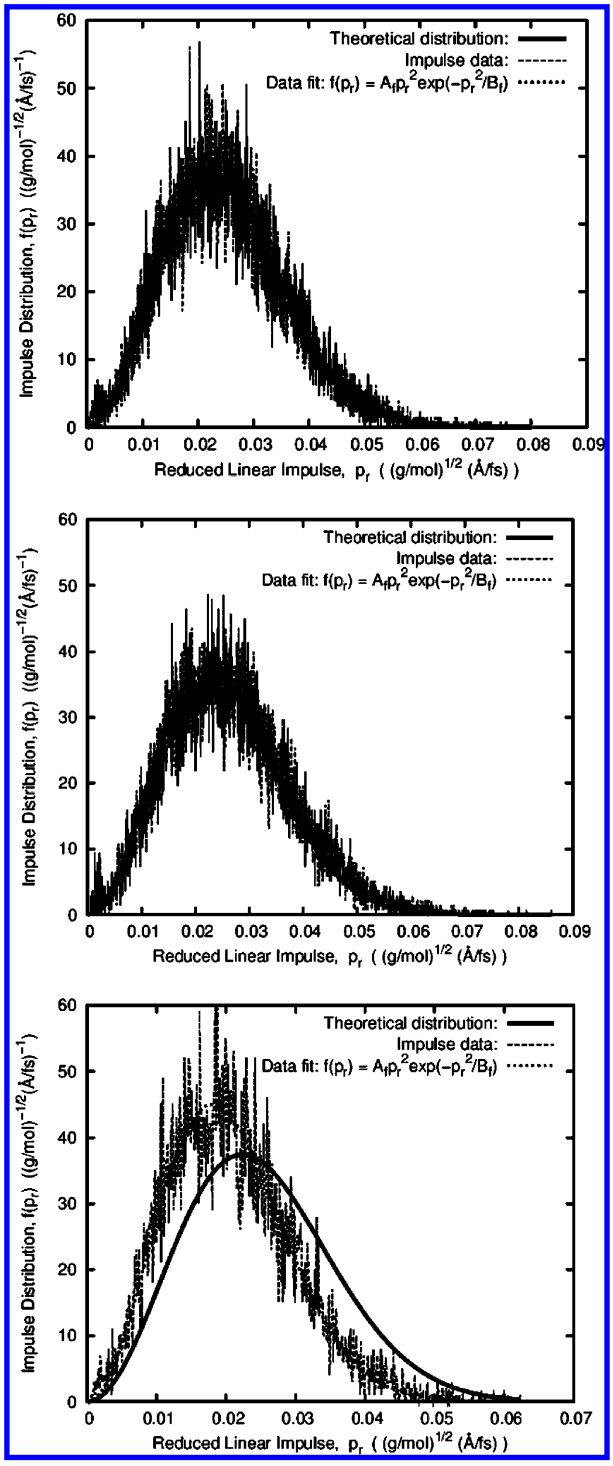

Figure 4. Distributions of the reduced linear impulses: 4 × C_{60} (top), z-car wheels (middle), z-car chassis (bottom).

with

$$\mathbf{n}_i = \frac{\mathbf{w}_i}{|\mathbf{w}_i|} \qquad \mathbf{n}_{\text{av}} = \frac{\sum_{i=1}^{4} \mathbf{n}_i}{|\sum_{i=1}^{4} \mathbf{n}_i|} \tag{15}$$

The possible numerical values for this function range from 0 (no correlations) to 1 (very strong correlations). The correlations in the absolute values of the angular velocities can be measured with the help of another function:

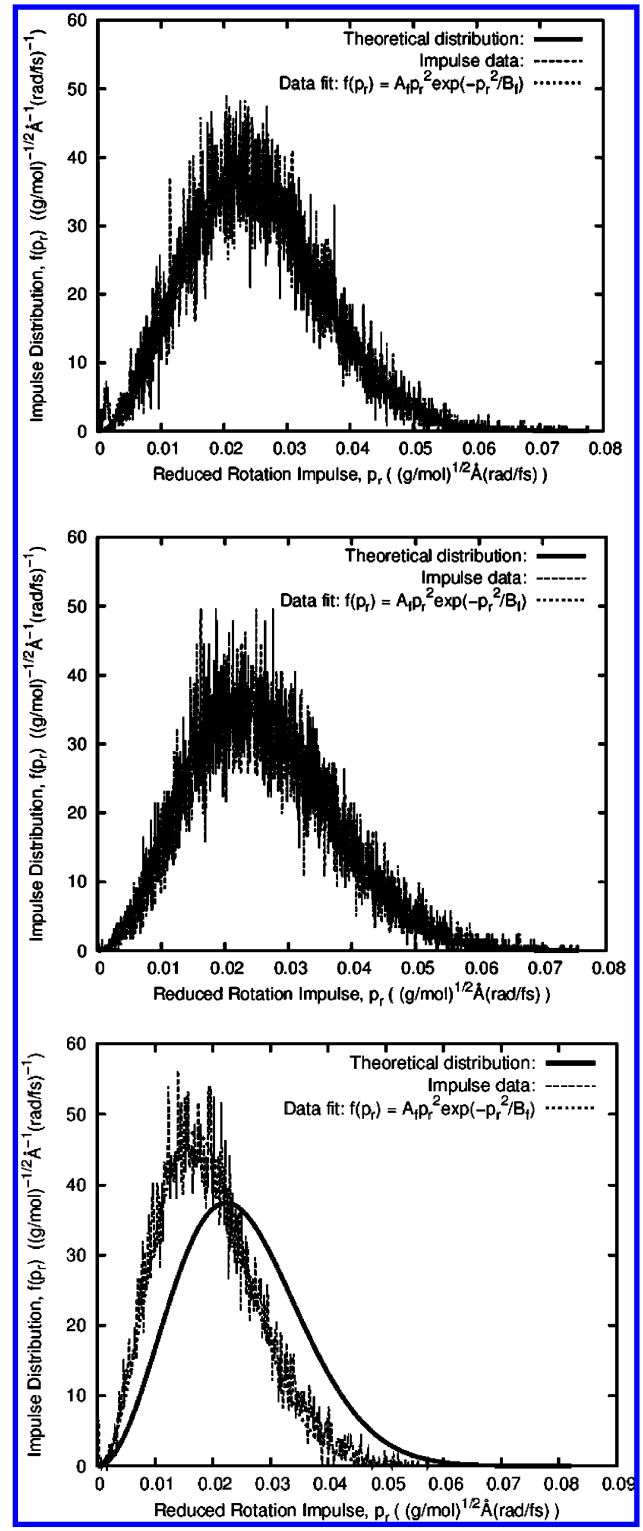

Figure 5. Distributions of the reduced rotational impulses: 4 × C_{60} (top), z-car wheels (middle), z-car chassis (bottom).

$$C_{\text{abs}} = \frac{\sqrt{\sum_{i=1}^{4} (|\mathbf{w}_i| - \overline{|w|})^2}}{\overline{|w|}} \qquad \overline{|w|} = \frac{1}{4}\sum_{i=1}^{4} |\mathbf{w}_i| \tag{16}$$

Typical temporal dependencies of the correlation functions are presented in Figures 6−8, and the averaged distributions of the values are given in Tables 2 and 3. All functions start from 0 since at $t = 0$ it is assumed that there are no

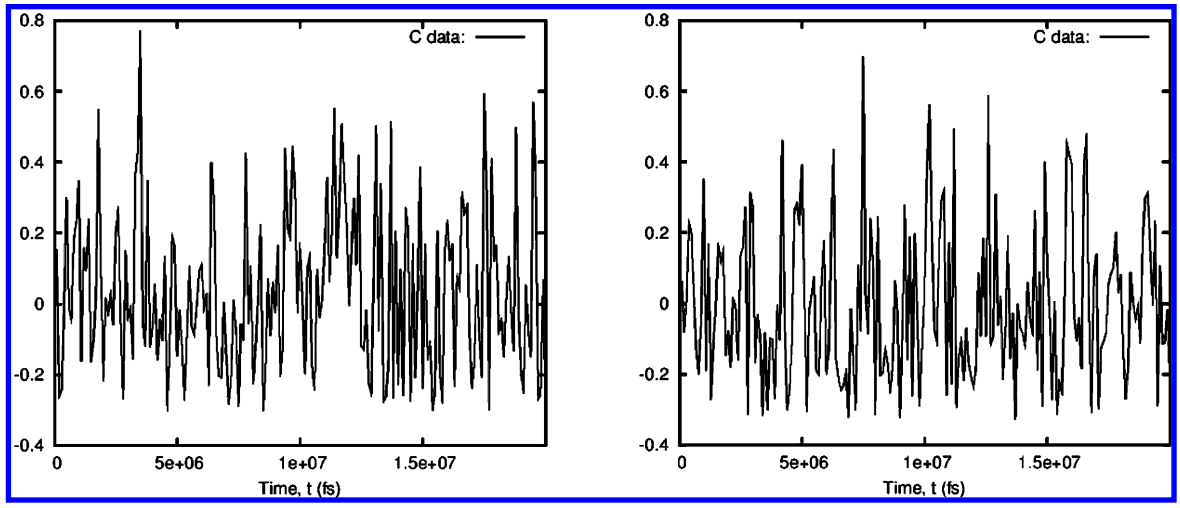

Figure 6. Typical temporal dependences of the correlation function C (eq 13) for the 4 × C_{60} system (left) and for the z-car (right).

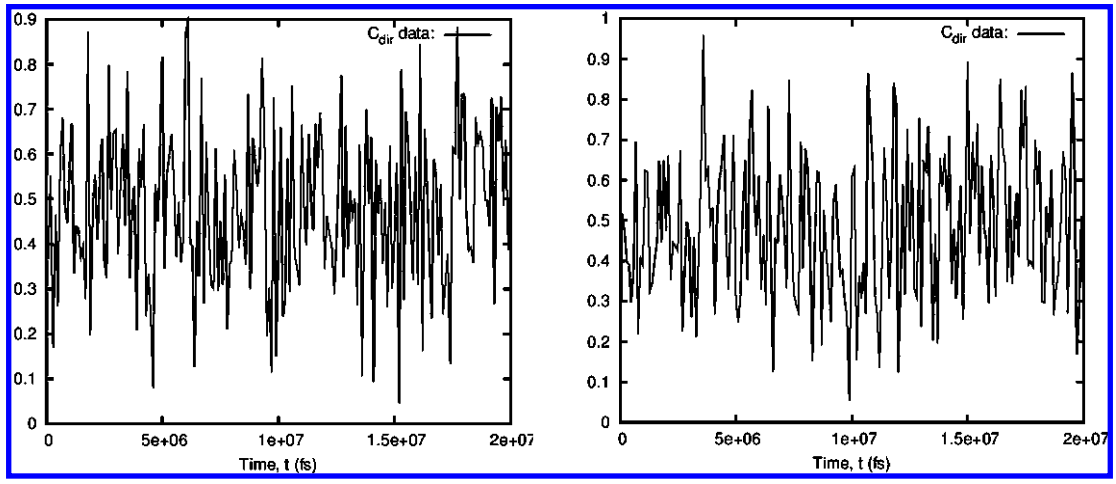

Figure 7. Typical temporal dependences of the correlation function C_{dir} (eq 14) for the 4 × C_{60} system (left) and for the z-car (right).

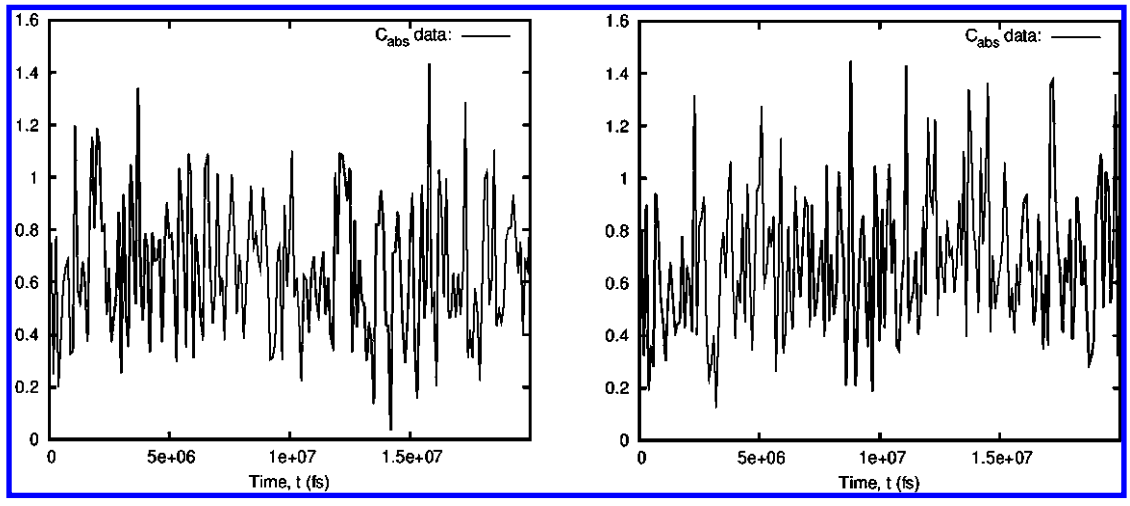

Figure 8. Typical temporal dependences of the correlation function C_{abs} (eq 16) for the 4 × C_{60} system (left) and for the z-car (right).

correlations. It is interesting to note that correlations in the wheels of the z-car molecule are similar to those of four separate fullerene wheels. Our results indicate that correlations in the motion of the wheels of the nanocars are small but not negligible. This is the result of complex interactions between different fragments of the molecule and interactions with the surface.

3.3. Mobility of Nanocars. Experimental and theoretical studies indicate that nanocars move stochastically along the surfaces. Their mobility could be quantized by analyzing

Table 2. Distribution C (Eq 13) for the Systems 4 × C_{60} and z-car

system	$0 \le C < 1/4$	$1/4 \le C < 1/2$	$1/2 \le C < 3/4$	$3/4 \le C < 1$
4 × C_{60}	0.121	0.452	0.356	0.071
z-car	0.121	0.468	0.344	0.067

Table 3. Distributions C_{dir} (Eq 14) and C_{abs} (Eq 16) for the Systems 4 × C_{60} and z-car

system	C_{dir}	$\Delta C_{dir}/C_{dir}$, %	C_{abs}	$\Delta C_{abs}/C_{abs}$, %
4 × C_{60}	0.469	0.4	0.679	0.4
z-car	0.465	0.4	0.686	0.4

Table 4. Comparison of Translational and Rotational Diffusion Coefficients

system	D_{trans}, Å^2 fs^{-1}	$\Delta D_{trans}/D_{trans}$, %	D_{rot}, rad^2 fs^{-1}	$\Delta D_{rot}/D_{rot}$, %
4 × C_{60}	0.010	7	1.3×10^{-5}	12
z-car	0.015	10	2.2×10^{-5}	14

effective diffusion coefficients. In our RB MD simulations we measured rotational diffusion following the change of the angle of rotation around the axis perpendicular to the surface:

$$D_{rot} = \frac{\varphi_{max}^2}{4t_{max}} \tag{17}$$

where $t_{max} = 2 \times 10^7$ fs. In a similar way, we can estimate the translational diffusion constants for different particles:

$$D_{trans} = \frac{r_{max}^2}{4t_{max}} \tag{18}$$

where $t_{max} = 2 \times 10^7$ fs and r_{max} is the position of the particle at the end of the trajectory, assuming that it started at the origin. Rotational and translational diffusion constants for different surfaces are presented in Table 4. Comparing the results for the z-car molecule and for the cluster of four fullerene molecules, which are quite close, one could argue that the most important factor controlling the dynamics of nanocars is their interactions with the surface and overcoming the barriers created by this potential energy and not interfragment interactions. However, we should be careful in this situation since in this system interactions between different parts of the molecule are relatively small. However, this conclusion might change for stronger interfragment interactions.

3.4. Effect of Molecular Flexibility. Since in the RB MD method it is possible to divide the molecule into different sets of fragments, we can investigate the question of how molecular flexibility affects the overall dynamics. For the motion of the z-car on the silver surface we analyzed five different ways of fragmentation for the same molecule. Our most flexible molecule has five fragments (four wheels and a chassis), while in other cases we combined some wheels into one rigid fragment with the chassis. Thus, we analyzed molecules with four, three, two, one, and zero rotating wheels. Translational diffusion coefficients, computed as discussed above, as functions of the number of fragments are shown in Figure 9. It can be seen that the diffusion constant is mostly an increasing function of the number of wheels that can rotate, although the results are quite noisy. This suggests that the rotation of fullerene wheels makes a significant contribution to the overall mobility of the z-car molecule. This can be understood using the following arguments. If all wheels are frozen, when the molecule is viewed as one rigid fragment, the only way it can move is by hopping on the surface. Allowing some wheels to rotate increases the overall mobility.

We also investigated the effect of the temperature on the mobility of the z-car molecule on the silver surface by performing RB MD at different temperatures. The results have been fitted in the standard Arrhenius expression

$$D = D_0 \exp\left[-\frac{E_a}{RT}\right] \tag{19}$$

where E_a is an effective activation energy. The activation energy as a function of the number of fragments has a nonmonotonic dependence: first it increases strongly, and then it slowly decreases (Figure 9a). We can propose the following explanation for this complex behavior. The smallest activation barrier is observed for the molecule without rotating wheels. When some wheels start to rotate, the molecule can adjust itself on the surface and find a lower minimum on the potential surface, something that the totally rigid molecule cannot do. Then it is harder for this molecule with few rotating wheels to hop because it takes more energy to overcome the larger barrier. However, increasing the number of rotating wheels also increases the contribution of rotations in the translational motion, which have smaller activation barriers.

Figure 9b also shows the effect of increasing the number of fragments of the nanocar molecule on the pre-exponential term in eq 19. Increasing the molecular flexibility strongly increases this parameter. These results can be easily understood. The pre-exponential factor describes the attempt frequency, and the more flexible molecule explores a larger phase space, allowing more attempts for the molecule to diffuse along the surface.

3.5. Comparison of Different Surfaces. In our simulations we have investigated the motion of nanocars on gold and silver surfaces. The dynamics in both cases are similar, but there are many differences. The potential used in the case of the gold surface has been obtained from CHARMM and from UFF force fields, while in the case of silver a combination of UFF and an empirically determined potential[38] has been used. The obtained parameters in both cases are comparable, with the exception of one. The equilibrium angle in the connection between the fullerene wheel and the chassis for the Ag surface was taken to be 120°. This is because the aromatic carbon has been utilized in these simulations on the silver surface. However, on the Au surface this angle was taken as 180°, corresponding to sp hybridization of the carbon atom. This difference leads to slightly different structures: the z-car molecule on the silver surface has a bend in the joint region of the wheels and chassis, while on the gold surface there is no such bend. As a result, the wheels are interacting stronger with the silver surface,

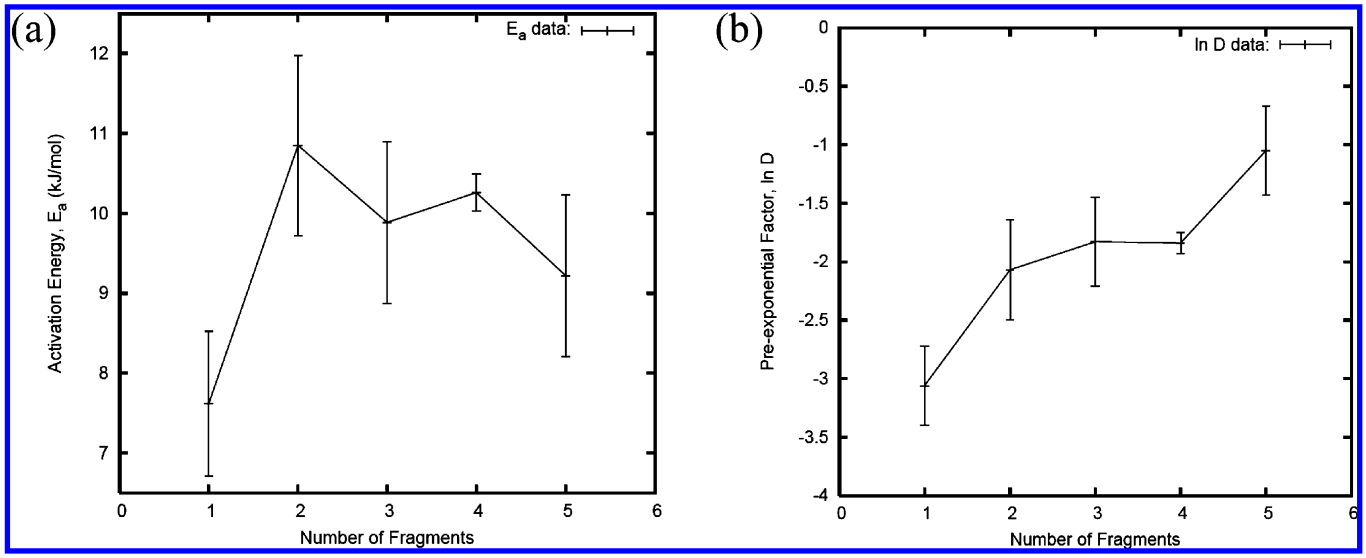

Figure 9. Activation energies (left) and pre-exponential factors (right) for diffusion of the z-car as a function of its flexibility.

leading to smaller diffusion coefficients. It will be interesting to test experimentally whether these theoretically predicted differences in the structures of the nanocars are real.

It is important to discuss how the electrostatic charges on a metal surface might influence our MD simulations. As was discussed above, to describe Ag−fullerene interactions, we have used an empirically found potential.[38] Since this potential provides reasonable adsorption energies for a series of molecules on the silver surface, the effect of charges is already implicitly included in our calculations. For fullerene−Au interactions the charge transfer plays an important role, and in general, it cannot be neglected. However, to not make our calculations very complex, we have neglected the electrostatic effects in this case because we are interested in more qualitative features of the dynamics that can be obtained without this contribution.

3.6. Comparison to the All-Atom MD Models. It is instructive to estimate the effects of the rigid-body restrictions on the dynamical behavior in these systems by comparing our results with those of the standard all-atom MD simulations. First, we reproduced the data from the work of Yoon et al.[44] in which the diffusion of gold clusters on graphite surfaces has been modeled. We considered one of the model systems, namely, the 140-atom gold cluster on a graphite surface (111), and precisely the same interaction potential parameters as in the original paper.[44] The diffusion coefficients have been computed in the all-atom MD simulations in complete agreement with the values reported in ref 44 and then for the modified model system in which the metal cluster was treated as a rigid body. We found that in the latter case the computed diffusion coefficients have been calculated to be approximately 1 order of magnitude larger than in the all-atom case. Qualitatively the same conclusion on larger values of diffusion coefficients estimated within the rigid-body MD simulations compared to the all-atom MD simulations has been obtained for another model system, the single C_{60} molecule on the Au(111) surface. Calculations of trajectories and estimates of the translational diffusion coefficients for the RB dynamics have been carried out as for other fullerene-based systems described above. To perform all-atom MD simulations, we considered five layers of gold atoms with the periodical cell of $20 \times 20 \times 100$ Å. The lowest layer has been frozen, and the four upper levels were allowed to be flexible as consistent with the Lennard-Jones parameters for Au−Au interactions $\varepsilon = 10.6$ kcal/mol and $\sigma = 2.57$ Å. The MM3 force field parameters were used to describe the all-atom C_{60} molecule. The obtained diffusion coefficient was approximately 2 orders of magnitude smaller than that estimated in the rigid-body simulations.

Therefore, we can conclude that approximations of RB MD for the fullerene-base nanocars on metal surfaces may account for somewhat faster dynamics as compared to the more accurate all-atom models. The diffusion coefficients estimated in the rigid-body simulations may be 1 or 2 orders larger due to restrictions imposed on the models.

Summary

We have investigated the reliability of RB MD computer simulation methods by analyzing the dynamics of nanocars on gold and silver surfaces. Several problems and issues have been analyzed.

The consequences of utilizing the Nosé−Poincaré thermostat are carefully studied at different conditions. It is found that numerical integration errors do not contribute significantly to determination of the dynamic properties of the system. However, if the trend in errors of measuring quantities continues, it might limit the length of time trajectories that can be used reliably for calculations of properties of the molecules on the surface. The way to improve the accuracy of the RB MD method is to have molecules pre-equilibrated or to neglect early times. In addition, this thermostat is consistent in reproducing canonical ensemble distributions. Thus, the application of the Nosé−Poincaré thermostat is an important part of RB MD simulations that allows this method to be realistic in computing the dynamic properties of the system.

The correlations in the motion of the wheels have been consistently analyzed via several correlation functions. It is found that these correlations are small, but they cannot be neglected.

In addition, we studied the effect of interactions, molecular flexibility, and temperature on the dynamics of single molecules hopping on surfaces. In the case of stronger interactions of the z-car molecule with the surface in comparison with interfragmental forces, these interactions fully determine all dynamic properties. It is also observed that increasing the flexibility raises the overall molecular mobility due to adding the contribution of the rotational motion to the ability to displace the molecule. We have found that the diffusion of nanocars is a temperature-activated process. The activation energy barrier shows a nonmonotonic dependence on the number of rigid fragments used in the simulations. This result is explained by interplay between two factors: increasing the number of fragments leads to more rotations, lowering the effective activation barrier, but individual rotations also allow the fragments to adjust to interact better with the surface, increasing the activation barrier. We also compared dynamical properties of nanocars on the gold and silver surfaces. It is argued that the z-car probably moves faster on Au because on the silver surface the wheels of the molecules are in bent configurations, leading to stronger interactions with the surface and slower overall motion.

Thus, our comprehensive analysis of RB MD computer simulation methods shows that this is a very reliable and highly convenient approach that might be successfully used for understanding the dynamics of nanoscale processes. However, it should be noted also that our calculations indicate that the rigid-body approximation leads to faster dynamics with larger diffusion coefficients (1−2 orders of magnitude) as compared with full atomic MD computer simulations. It will be interesting to extend this approach to describe systems under the effect of external fields (electromagnetic, light, etc.), systems on different surfaces, including nonmetallic, and systems with many moving and interacting species.

Acknowledgment. A.B.K. acknowledges support from the Welch Foundation (Grant C-1559) and from the U.S. National Science Foundation (Grant ECCS-0708765). This work was also supported in part by the Shared University Grid at Rice University and by the Russian Foundation for Basic Research (Grant 09-03-00338). The Russian team acknowledges the facilities of the Supercomputing Complex of the Research Computing Center of M.V. Lomonosov Moscow State University and the SKIF-GRID program for providing computational resources.

References

(1) Dominguez, Z.; Dang, H.; Strouse, J.; Garcia-Garibay, M. A. *J. Am. Chem. Soc.* **2002**, *124*, 2398.

(2) Godinez, C. E.; Zepeda, G.; Garcia-Garibay, M. A. *J. Am. Chem. Soc.* **2002**, *124*, 4701.

(3) Kottas, G. S.; Clarke, L. I.; Horinek, D.; Michl, J. *Chem. Rev.* **2005**, *105*, 1281.

(4) Balzani, V.; Credi, A.; Venturi, M. *ChemPhysChem* **2008**, *9*, 202.

(5) van Delden, R. A.; ter Wiel, M. K. J.; Pollard, M. M.; Vicario, J.; Koumura, N.; Feringa, B. L. *Nature* **2005**, *437*, 1337.

(6) Gimzewski, J. K.; Joachim, C.; Schlittler, R. R.; Langlais, V.; Tang, H.; Johannsen, I. *Science* **1998**, *281*, 531.

(7) Baber, A. E.; Tierney, H. L.; Sykes, E. C. H. *ACS Nano* **2008**, *2*, 2385.

(8) Michl, J.; Sykes, E. C. H. *ACS Nano* **2009**, *3*, 1042.

(9) Vives, G.; Kang, J.; Kelly, K. F.; Tour, J. M. *Org. Lett.* **2009**, *11*, 5602.

(10) Claytor, K.; Khatua, S.; Guerrero, J.; Tcherniak, A.; Tour, J. M.; Link, S. *J. Chem. Phys.* **2009**, *130*, 164710.

(11) Khatua, S.; Guerrero, J. M.; Claytor, K.; Vives, G.; Kolomeisky, A. B.; Tour, J. M.; Link, S. *ACS Nano* **2009**, *3*, 351.

(12) Vives, G.; Tour, J. M. *Acc. Chem. Res.* **2009**, *42*, 473.

(13) Vives, G.; Tour, J. M. *Tetrahedron Lett.* **2009**, *50*, 1427.

(14) Sasaki, T.; Guerrero, G.; Leonard, A. D.; Tour, J. M. *Nano Res.* **2008**, *1*, 412.

(15) Shirai, Y.; Morin, J.-F.; Sasaki, T.; Guerrero, J. M.; Tour, J. M. *Chem. Soc. Rev.* **2006**, *35*, 1043.

(16) Shirai, Y.; Osgood, A. J.; Zhao, Y.; Yao, Y.; Saudan, L.; Yang, H.; Yu-Hung, C.; Sasaki, T.; Morin, J.-F.; Guerrero, J. M.; Kelly, K. F.; Tour, J. M. *J. Am. Chem. Soc.* **2006**, *128*, 4854.

(17) Akimov, A. V.; Nemukhin, A. V.; Moskovsky, A. A.; Kolomeisky, A. B.; Tour, J. M. *J. Chem. Theory Comput.* **2008**, *4*, 652.

(18) Reich, S. *SIAM J. Numer. Anal.* **1996**, *33*, 475.

(19) Ikeguchi, M. *J. Comput. Chem.* **2004**, *25*, 529.

(20) Miller III, T. F.; Eleftheriou, M.; Pattnaik, P.; Ndirango, A.; Newns, D.; Martyna, G. J. *J. Chem. Phys.* **2002**, *116*, 8649.

(21) Omelyan, I. P. *Phys. Rev. E* **1998**, *58*, 1169.

(22) Omelyan, I. P. *Comput. Phys. Commun.* **1998**, *109*, 171.

(23) Moskovsky, A. A.; Vanovschi, V. V.; Konyukhov, S. S.; Nemukhin, A. V. *Int. J. Quantum Chem.* **2006**, *106*, 2208.

(24) Dullweber, A.; Leimkuhler, B.; McLachlan, R. *J. Chem. Phys.* **1997**, *107*, 5840.

(25) Tierney, H. L.; Baber, A. E.; Sykes, E. C. H.; Akimov, A.; Kolomeisky, A. B. *J. Phys. Chem. C* **2009**, *113*, 10913.

(26) Horinek, D.; Michl, J. *Proc. Natl. Acad. Sci. U.S.A.* **2005**, *102*, 14175.

(27) Horinek, D.; Michl, J. *J. Am. Chem. Soc.* **2003**, *125*, 11900.

(28) Hou, S.; Sagara, T.; Xu, D.; Kelly, T. R.; Ganz, E. *Nanotechnology* **2003**, *14*, 566.

(29) Vacek, J.; Michl, J. *Adv. Funct. Mater.* **2007**, *17*, 730.

(30) Bond, S. D.; Leimkuhler, B. J.; Laird, B. B. *J. Comput. Phys.* **1999**, *151*, 114.

(31) Nosé, S. *J. Chem. Phys.* **1984**, *81*, 511.

(32) Nosé, S. *J. Phys. Soc. Jpn.* **2001**, *70*, 75.

(33) Leimkuhler, B. L.; Sweet, Ch. R. *J. Chem. Phys.* **2004**, *121*, 108.

(34) Martyna, G. J.; Klein, M. L.; Tuckerman, M. *J. Chem. Phys.* **1992**, *97*, 2635.

(35) MacKerell, A. D., Jr.; Bashford, D.; Bellott, M.; Dunbrack, R. L., Jr.; Evanseck, J. D.; Field, M. J.; Fischer, S.; Gao, J.; Guo, H.; Ha, S.; Joseph-McCarthy, D.; Kuchnir, L.; Kuczera, K.; Lau, F. T. K.; Mattos, C.; Michnick, S.; Ngo, T.; Nguyen, D. T.; Prodhom, B.; Reiher, W. E., III; Roux, B.; Schlenkrich, M.; Smith, J. C.; Stote, R.; Straub, J.; Watanabe, M.;

Wiórkiewicz-Kuczera, J.; Yin, D.; Karplus, M. *J. Phys. Chem. B* **1998**, *102*, 3586.

(36) Foloppe, N.; MacKerell, A. D., Jr. *J. Comput. Chem.* **2000**, *21*, 86.

(37) Rappe, A. K.; Casewit, C. J.; Colwell, K. S.; Goddard, W. A., III; Skiff, W. M. *J. Am. Chem. Soc.* **1992**, *114*, 10024.

(38) Jalkanen, J. P.; Zerbetto, F. *J. Phys. Chem. B* **2006**, *110*, 5595.

(39) Wang, L. L.; Cheng, H. P. *Phys. Rev. B* **2004**, *69*, 165417.

(40) Wang, L. L.; Cheng, H. P. *Phys. Rev. B* **2004**, *69*, 045404.

(41) Perez-Jimenez, A. J.; Palacios, J. J.; Louis, E.; SanFabian, E.; Verges, J. A. *ChemPhysChem* **2003**, *4*, 388.

(42) Tzeng, C. T.; Lo, W. S.; Yuh, J. Y.; Chu, R. Y.; Tsuei, K. D. *Phys. Rev. B* **2000**, *61*, 2263.

(43) Rogero, C.; Pascual, J. I.; Gomez-Herrero, J.; Baro, A. M. *J. Chem. Phys.* **2002**, *116*, 832.

(44) Yoon, B.; Luedtke, W. D.; Gao, J.; Landman, U. *J. Phys. Chem. B* **2003**, *107*, 5882.

CT100101Y